Bio-Design and Manufacturing (2023) 6:255–267
https://doi.org/10.1007/s42242-022-00221-3

RESEARCH ARTICLE

Multidrug dissolvable microneedle patch for the treatment of recurrent oral ulcer

Yuqiong Wang[1] · An'an Sheng[1,2] · Xinran Jiang[1] · Shanshan Yang[1,2] · Long Lin[1,3] · Mingzhu Yang[4] · Fengshuo Zhu[5] · Yongyan Hu[6] · Jian Li[2] · Lingqian Chang[1]

Received: 10 March 2022 / Accepted: 7 November 2022 / Published online: 28 December 2022

Abstract

Recurrent oral ulcer is a painful oral mucosal disorder that affects 20% of the world's population. The lack of a radical cure due to its unknown underlying cause calls for innovative symptomatic treatments. This work reports a hyaluronic acid-based dissolvable microneedle patch (ROUMN patch, short for recurrent oral ulcer microneedle) loaded with dexamethasone acetate, vitamin C and tetracaine hydrochloride for the treatment of recurrent oral ulcers. The ROUMN patch shows enhancement in both the anti-inflammatory effect elicited by dexamethasone and the pro-proliferation effect of vitamin C. In vitro experiments show that ROUMN has a higher efficiency in suppressing lipopolysaccharide (LPS)-induced interleukin-6 (IL-6) expression than dexamethasone alone. Cell proliferation and migration were also significantly promoted by ROUMN compared to vitamin C alone. The healing-promoting effect of ROUMN was also verified in vivo using an acetic acid-cauterized oral ulcer model in rats. ROUMN as a treatment accelerated the healing process of oral ulcers, shortening the total healing time to 5 days compared with the 7 days required by treatment using watermelon frost, a commonly used over-the-counter (OTC) drug for oral ulcers. The rapid dissolution of the hyaluronic acid-based microneedles and the superior healing-promoting effect of the drug combination could lead to a broad application prospect of the ROUMN patch in the treatment of recurrent oral ulcers.

Yuqiong Wang, An'an Sheng, Xinran Jiang, and Shanshan Yang have contributed equally to this work.

✉ Yongyan Hu
huyyg@163.com

✉ Jian Li
riken@xmu.edu.cn

✉ Lingqian Chang
lingqianchang@buaa.edu.cn

[1] Beijing Advanced Innovation Center for Biomedical Engineering, School of Biological Science and Medical Engineering, Beihang University, Beijing 100191, China

[2] Department of Stomatology, Xiang'an Hospital of Xiamen University, Xiamen 361000, China

[3] Institute of Plastic Machinery and Plastic Engineering, School of Mechanical and Electrical Engineering, Beijing University of Chemical Technology, Beijing 100029, China

[4] Department of Biochemistry, Institute of Basic Medical Sciences, Chinese Academy of Medical Sciences (CAMS) and Peking Union Medical College, Beijing 100005, China

[5] Department of Oral Maxillofacial-Head and Neck Oncology, Shanghai Ninth People's Hospital, Shanghai 200011, China

[6] Laboratory Animal Facility, Peking University First Hospital, Beijing 100034, China

Graphic abstract

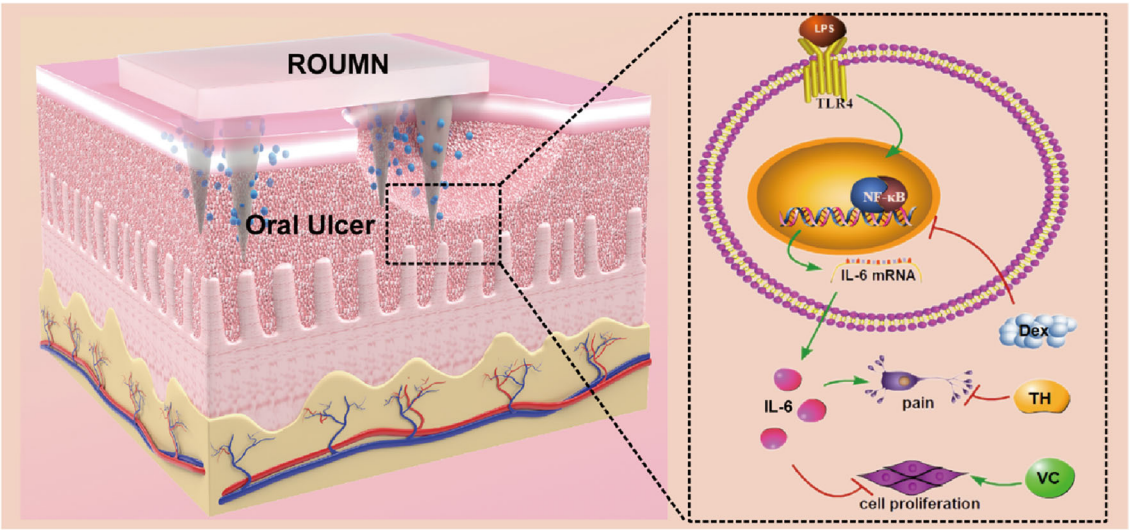

Keywords Recurrent oral ulcer · Dissolvable microneedle · Hyaluronic acid microneedle · Multidrug · Anti-inflammation · Healing promoting effect

Introduction

Oral ulcer (aphthous stomatitis), or canker sore, is the most common oral mucosa disorder that affects 20% of the world population [1, 2]. The clinical manifestation of an oral ulcer is a round- or oval-shaped superficial defect of the local mucosa covered with a gray–white pseudomembrane [1, 2]. The central concavity of the ulcer is surrounded by an erythematous halo [3, 4]. Due to the abundant distribution of nerves in the oral mucosa, the progression of ulceration is usually accompanied by spontaneous burning sensations and pain, and worsens upon stimulation. Since ulcers have a clinical progression that usually lasts for 1–2 weeks and recurs easily, this oral disorder disturbs the patient's life to varying degrees [1, 3]. As the cause of oral ulcers is complex and no radical cure exists to date, local medication for pain relief is common, and symptomatic treatment, such as medication to promote ulcer healing, is recommended as a first-line treatment [1, 2, 5].

At present, drugs used for local treatment of recurrent oral ulcers (ROU) include the following categories: corticosteroids, antimicrobials, drugs that promote healing, and anesthetics [1, 6]. The above drugs are often applied to the local mucosa in the form of mouthwash, topical paste, buccal tablet/film or spray [1, 5, 7, 8]. However, drug concentration may be diluted by the saliva, and buccal tablets and topical pastes that are designed to work as lesion adhesives may detach from the lesion as the masticatory muscles move. Additionally, as the pseudomembrane over the ulcer poses a physical barrier to local drug penetration, the residence time of the drugs in contact with the lesion could be too short to ensure clinical efficacy.

To better penetrate the pseudomembrane that is composed mainly of necrotic epithelial cells, debris and fibrin [1] and achieve steady release of drugs at unimpaired concentrations, we constructed a drug-loaded dissolvable microneedle (MN) patch for the treatment of ROU. The recurrent oral ulcer microneedle (ROUMN) patch adopts hyaluronic acid (HA) as the base material and carries three functional drugs, dexamethasone acetate (Dex), vitamin C (VC) and tetracaine hydrochloride (TH), for anti-inflammation, pro-proliferation and anesthetic purposes, respectively. As a naturally occurring polysaccharide in the human body, typically in the extracellular matrix, HA, especially of molecular weight 10–400 kDa, has widely been used to fabricate dissolvable microneedles for various transdermal treatments [9–11]. In addition to the fact that low molecular weight (20–300 kDa) HA naturally participates in the biological process of wound healing or significantly improves wound closure, HA's remarkable water-retaining ability makes it ideal for application in the moist environment of the oral cavity [12–14]. Dexamethasone is a glucocorticoid that is typically used in the wound healing context for decreased inflammation [15, 16]. It has been clinically tested to safely promote the healing of recurrent oral ulcers as a topical treatment, with an additional pain-relief effect [6]. Vitamin C (ascorbic acid) has been clinically proven to promote oral wound and ulcer healing [17, 18]. The proliferative/regenerative effect of VC

is manifested especially towards connective tissues by contributing to the synthesis and cross-linking of collagen [19]. Tetracaine is an ester-type anesthetic agent that has been clinically proven to exhibit a long-lasting local anesthetic effect with a short application time when administered topically [20, 21]. MNs have been proven to be a painless, efficient transdermal drug delivery system [22, 23]; with anesthetic loading, ROUMNs should cause minimal stimulation of the ulcerated lesion and thus ensure the comfort and compliance of patients. With the optimal concentration of HA, ROUMN exhibits sufficient mechanical strength to effectively penetrate the pseudomembrane. The MN structure could fix the ROUMN patch securely onto the oral ulcer, resulting in an improved residence time of drugs compared with other topical agents. Meanwhile, rapid dissolution of the HA-based MNs allows for the release and distribution of the preloaded drugs from the ROUMN patch directly into the bottom of the ulcerated lesion for an accelerated therapeutic effect [24]. These advantages combined present a broad application prospect of ROUMN in the treatment of recurrent oral ulcers.

Materials and methods

Materials and instruments

Commercial reagents used in this study include 300 kDa hyaluronic acid (HA) (Macklin, 9004-61-9), polydimethylsiloxane (Sigma-Aldrich, 63148-62-9), tetracaine hydrochloride (TH) (9 Ding Chem, 136-47-0), vitamin C (VC) (ACMEC, L65552), dexamethasone acetate (Dex) (Macklin, D829854), fluorescein isothiocyanate (FITC) (Biofroxx, 2284MG050), methylene blue (Coolaber, CM7291), lipopolysaccharide (LPS) (CST, 14011S), rat interleukin-6 (IL-6) enzyme-linked immunosorbent assay (ELISA) kit (BOSTER, EK0421), rat tumor necrotic factor alpha (TNF-α) ELISA kit (GPL, P09R030), FastPure Cell/Tissue Total RNA Isolation Kit V2 (Vazyme, RC112-01), One Step TB Green® PrimeScript™ Reverse Transcriptase Polymerase Chain Reaction (RT–PCR) Kit (TaKaRa, RR066A), quantitative reverse transcriptase PCR (RT-qPCR) primers (Beijing RuiBiotech Co., Ltd.), Cell Counting Kit-8 (CCK-8) reagent (Dojindo, CCK-8), and IL-6 antibody (Abmart, IL-6 Antibody).

Instruments used in this study include a three-dimensional (3D) printer, nanoArch P140 high-precision printing system (BMF Material Technology Inc., Shenzhen, China); a universal testing machine, ESM303 Motorized Tension/Compression Test Stand & Series 5 Advanced Digital Force Gauge (MARK-10 Corporation, Copiague, USA); an optical coherence tomography machine, MOPTIM QSLF-1500 (Shenzhen Moptim Imaging Technique Co., Ltd., China); a transdermal diffusion tester, TP-6 Intelligent Transdermal Diffusion Tester (Tianjin Xinzhou Science and Technology Co., Ltd.); a plate reader, Spark® Multimode Microplate Reader (Tecan Trading AG, Switzerland); and a digital slide scanner, PANNORAMIC MIDI II (3DHISTECH Ltd., Budapest, Hungary).

Methods

Fabrication of dissolvable microneedle patch

The 3D model of the dissolvable microneedle patch was constructed using 3D Max 2018. The MN patch has a 0.5 cm× 0.5 cm patch base with an array of 10×10 cone-shaped MNs, and each MN has a height of 350 μm and a base diameter of 200 μm.

The designed model was then 3D printed (surface projection microstereolithography) with high temperature laminating (HTL) yellow-5 resin (photo-curing wavelength = 405 nm) using the nanoArch P140 high-precision printing system. The resin model was used as the template in the micromolding of all dissolvable microneedle patches used in this study. In brief, (1) the resin template was placed in a well of a 6-well plate. (2) Polydimethylsiloxane (PDMS) base and curing agent were stir-mixed in a 10:1 ratio by weight and then poured onto the resin prototype until the prototype was fully immersed. (3) The 6-well plate was placed in a vacuum pump to eliminate the air bubbles in the PDMS. (4) The 6-well plate was then placed in a drying oven at 60 °C for 1 h for PDMS to solidify. (5) The resin template was removed from the solidified PDMS mold with a blade. Two more PDMS molds were made by repeating the above steps, and each mold was used repeatedly for the fabrication of dissolvable microneedle patches. (6) For drugless HA microneedles, 0.0833 g 300 kDa HA powder was dissolved in 1 mL ultrapure water; for drug-loaded HA microneedle patches (i.e., ROUMN), 111 μL of 1 mM dexamethasone acetate solution, 58.6 μg vitamin C powder, and 5.5 mg tetracaine hydrochloride powder were added into the 1 mL HA solution. A 200 μL portion of base solution was filled into each micromold, resulting in 8.68 μg dexamethasone acetate, 10.54 μg vitamin C and 0.99 mg tetracaine hydrochloride in each ROUMN patch. For gelatin/starch microneedles, gelatin, starch and ultra-pure water were mixed at a 1:1:5 ratio (w/w) for the preparation of the microneedle base solution. The base solution was poured into the PDMS mold, vacuumed, centrifuged at 4000 r/min for 30 min at room temperature, and then dried in a drying oven at 37 °C to obtain the corresponding type of MN patches.

Mechanical test of dissolvable microneedle patches

Compression test: Flat-surfaced metal blocks were installed on the universal testing machine, and a ROUMN patch was taped on top of the bottom block with MNs facing upwards. The top block was moved downwards through the wired control panel. The distance between the two blocks was decreased by increments of 2 μm once the top block touched the MNs. MN displacement and the corresponding force applied were recorded by the computer.

Ex vivo penetration test: Two excisions of rat dorsal skin were immersed in phosphate-buffered saline (PBS), and then HA or gelatin/starch MN patches were pressed onto the skin excisions with a finger. The skin excisions were stained with methylene blue once the MN patches were removed and then taken under a microscope for observation.

In vivo penetration test: ROUMN was pressed into the ventral skin of anesthetized mice with hair thoroughly removed, and then the marks left by MNs were examined with an optical coherence tomography (OCT) machine after the ROUMN patch was removed.

Transdermal diffusion test of FITC-loaded dissolvable microneedles

Preparation of FITC-loaded dissolvable microneedles: 10 μL of 10 mg/mL FITC was added to 12 mL ultrapure water and mixed well; then, 1 g HA powder or 1 g 1:1 (w/w) gelatin-starch mixture was added to FITC solution and mixed well. The FITC-HA solution or FITC-gelatin/starch solution was poured into the PDMS mold and dried in a drying oven. The solidified microneedle patch was removed from the mold and trimmed to weigh 2 mg. Multiple microneedle patches were prepared.

Transdermal diffusion test: Sample flasks of the transdermal diffusion tester were filled with PBS and preheated to 37 °C in the reaction units. Dorsal skin was harvested from sacrificed mice, and hair was thoroughly removed. Once washed with saline 3 times, the skin was patted dry with a paper towel and fully spread on a plastic sheet. The skin was cut into 3 cm×3 cm pieces, and an FITC-HA and an FITC-gelatin/starch MN patch were pressed onto separate skin pieces. The MN patch was then firmly pressed with the glass stamp accessory, and the whole system was transferred and clipped onto the opening of a sample flask. The flask was put back into the reaction unit, and the magnetic stirrer was turned on. A 200 μL sample was extracted from each flask through the cannula with a pipet at 10, 20, 30, 45, and 60 min, respectively. PBS was added to the flasks after each sample extraction to keep the flask full. Samples were distributed in a black 96-well plate for fluorescence intensity measurement using the Spark® multimode microplate reader with the excitation wavelength set at 494 nm, emission wavelength at 518 nm, and bandwidth at 20 nm.

LPS-induced inflammation in rat aortic endothelial cells (RAECs)

LPS powder (1 mg) was completely dissolved in 1 mL complete Dulbecco's Modified Eagle Medium (cDMEM) in a 1.5 mL Eppendorf centrifuge tube to prepare a 1 mg/mL concentrated LPS solution. Two milliliters of 50, 10, 1 and 0.5 ng/mL LPS solution were then prepared from the 1 mg/mL concentrated LPS solution with cDMEM. Log phase RAECs were seeded into 96-well plates at 5×10^4 cells per well and incubated at 37 °C for 12 h. After 12 h, the seeded wells were divided into 5 groups and labeled, and the original culture medium was extracted. Two hundred microliters of cDMEM or 50, 10, 1, or 0.5 ng/mL LPS solution was added to each well of the 5 groups. After 4 h of incubation at 37 °C, 100 μL supernatant was extracted from each well for subsequent analysis.

ELISA measurement of IL-6 and TNF-α expressed by RAEC

Standard curves of IL-6 and TNF-α were plotted using the standard samples provided in the IL-6 or TNF-α ELISA kit, following the instruction manual. Preparation steps of the experimental samples are as follows:

(1) Dex acetate crystal (1 mg) was dissolved in 2.301 mL cDMEM to prepare a 1 mM Dex solution, which was then diluted with cDMEM to make 100 μM, 50 μM, and 10 μM Dex solutions. For the drug combination solution, 1 mg Dex, 0.7 mg VC and 0.4 mg TH were dissolved in 2.301 mL cDMEM. (2) Log phase RAECs were seeded in 96-well plates at a density of 5×10^4 cells per well. After 12 h of incubation, the original cell culture medium was removed; cells of the IL-6 group were treated with 100 μL of 10 ng/mL LPS solution for 2 h, and cells of the TNF-α group were treated with 100 μL of 500 ng/mL LPS solution for 24 h. After removing the LPS solution, the seeded wells of each group were divided into 5 subgroups and treated with 100 μL Dex solution or drug combination solution of 1 mM, 100 μM, 50 μM, 10 μM and 0 μM (cDMEM). After 24 h of treatment at 37 °C, the supernatant was collected for analysis.

Samples were read at 450 nm in the Spark® multimode microplate reader.

RT–qPCR detection of ROUMN regulation of LPS-induced IL-6 mRNA in RAEC

Primers used:
For rat *IL-6*: forward 5′-CACTTCACAAGTCGGAGGCT-3′, reverse 5′-TCTGACAGTGCATCATCGCT-3′; for rat

GAPDH: forward 5′-TGATTCTACCCACGGCAAGTT-3′, reverse 5′-TGATGGGTTTCCCATTGATGA-3′.

Log phase RAECs were seeded in 96-well plates at 5×10^5 cells/well and allowed to grow for 12 h. The wells were divided into two groups, where the LPS group was incubated with 100 μL 10 ng/mL LPS cDMEM and the control group with 100 μL cDMEM. After 4 h of incubation, the original medium was discarded, and both groups were divided into three subgroups, treated with 100 μL 1 mM Dex cDMEM, ROUMN with an equivalent amount of Dex in 100 μL cDMEM and blank cDMEM. The cells were incubated for 24 h. The cells were then trypsinized and collected for total RNA extraction using the Vazyme RNA isolation kit. Total RNA was analyzed by RT–qPCR using the TaKaRa One Step RT–PCR Kit and the above primers.

CCK-8 assay

Log phase RAECs were seeded in a 96-well plate at 1×10^4 cells per well and incubated at 37 °C for 24 h with 10, 50, 100, 200 or 300 μM VC solution or drug combination (Dex, VC and TH) solution with the same concentration gradient of VC. CCK-8 solution was mixed with serum-less DMEM at a ratio of 1:10, and 100 μL of the mixture was added to the plate per well. After 1 h of incubation, the 96-well plate was taken for measurement of absorbance at 450 nm in the Spark® multimode microplate reader. The measured values of absorbance were then converted to percentage cell viability based on the blank sample (treated with PBS).

Scratch assay

Log phase RAECs were seeded into three 5 cm^2 Petri dishes at 5×10^5 cells/mL and incubated at 37 °C. After 12 h, the original culture medium was replaced with 2 mL cDMEM, 2 mL 300 μM VC-supplemented cDMEM, or 2 mg ROUMN patch in 2 mL cDMEM. After 24 h of incubation at 37 °C, the solutions in the Petri dishes were replaced with 2 mL of 5 μM calcein AM in cDMEM. After a 30 min incubation for staining, a 1000 μL pipet tip was used to create the scratch in each Petri dish. The calcein AM solution was discarded, the cells were washed with PBS 3 times, and then 2 mL of cDMEM was added to each dish. The Petri dishes were incubated at 37 °C after images of the scratches were taken with a fluorescence. Images were taken again after 24 h of incubation, and the area of the scratches was compared between the two time points within each group. Area analysis was performed with ImageJ.

Animal experiment

All rats used in this work were anesthetized by intraperitoneal injection of 2% pentobarbital sodium at 50 mg/kg before undergoing any surgical operations. The mice used in this work were gas-anesthetized with isoflurane with a chamber output of 0.5 and a mask output of 1.0.

Model establishment: on day 0, a cotton swab was immersed in 99.9% acetic acid until fully saturated and then pressed against the buccal mucosa of the anesthetized rat. For each individual ulcer created, a new cotton swab was used, and the pressing remained for 2 min. The morphology of the oral ulcers was recorded on day 1 as the initial state.

Experimental procedure: On each day from day 1 to day 5, the morphology of the oral ulcers was first recorded, and then treatments were applied once per day. In each rat, the upper left ulcer was left untreated as the negative control; the upper right ulcer was treated with a 2 mg ROUMN patch (ROUMN group); the lower left ulcer was treated with a 2 mg drug-loaded patch without MNs (Patch group), and the lower right ulcer was treated with 2 mg watermelon frost powder (WF group). The morphology of the ulcers was recorded daily from day 6 to day 9, and no treatments were applied.

Behavioral test: Three mice were anesthetized in a chamber gassed with isoflurane; once the dorsal skin was exposed with an electric shaver and hair removal cream, two ulcers were created with a 99.9% acetic acid-saturated cotton swab on each mouse on each side of the spine in the waist area while the mouse remained under gas anesthesia through the mask. Before removing the mask, a ROUMN patch was pressed onto the right-side ulcer, and an MN patch without TH (the control group) was pressed onto the left-side ulcer on each mouse. Once the mice woke up from anesthesia, the number of times that each mouse licked the ulcer on each side was recorded for 45 min (when all control group MN patches detached from the skin), and the time points of MN patch detachment were also recorded for both groups.

Immunostaining

Tissues harvested from the rat oral cavity were fixed with formalin and embedded in paraffin. Paraffin slides were sectioned at 4 μm. For hematoxylin & eosin (H&E) staining, the slides were stained with hematoxylin and eosin, dehydrated with an ascending gradient of ethanol, and then deparaffinized with xylene. For immunohistochemistry staining, the slides were deparaffinized with xylene and rehydrated with a descending gradient of ethanol. The slides were then heated in a microwave with citrate buffer for antigen retrieval and blocked with 1.5% normal goat serum. Incubation with primary antibody (IL-6, 1:300 dilution) at 4 °C overnight was followed by secondary antibody incubation at room temperature. Finally, the slides were stained with diaminobenzidine and hematoxylin and dehydrated with ethanol.

Image analysis

All H&E and immunohistochemistry slides were scanned using the PANNORAMIC MIDI II digital slide scanner. In the H&E staining images, the basal layer of the surrounding healthy tissue was taken as the baseline for ulcer depth analysis. The perpendicular distance from the baseline to the level of the deepest point of the ulcer was calculated using ImageJ. In the immunohistochemistry images, the positive rate of IL-6 was calculated as the percentage of the brownish area within all epithelial layers above the lamina propria using ImageJ.

Results and discussion

Overall design and fabrication of ROUMN

The ROUMN patch is designed to effectively cover the entire ulcerated lesion, including the congested area, while ensuring that the MN tips pierce through the ulcer and reach the basal layer (Fig. 1a). As the study of ROU treatment requires a rat model for enough operational space in the oral cavity, we established a rat oral ulcer model, and the length of the MNs of the ROUMN patch was customized to fit the parameters of the model. After analyzing 3 samples of the ulcerated tissue, a length of 350 μm was chosen to cover the maximal depth of the rat oral ulcer model (Fig. S1 in Supplementary Information) so that the drug molecules distribute across the entire ulcerated lesion once the MNs dissolve. Treatment of oral ulcers also requires the MNs applied to bear certain characteristics: (1) a relatively high dissolution and diffusion rate to ensure direct and local drug distribution across the ulcerated area before the position of the MN patch is disrupted by mouth movement or saliva secretion; (2) fine needle tips and sufficient mechanical strength to penetrate the oral mucosa; (3) the oral application scenario also requires the patch base to bear a certain level of flexibility so that it is bendable upon application to fit the rugged surface of the oral cavity and minimize the sensation of foreign bodies in the mouth to enhance patient compliance. Based on these requirements, we screened through different types of dissolvable and biodegradable polymers in the early stage of this work, and HA was selected as the base material of ROUMN, as it shows favorable quality in all three characteristics required in fabricating the MN patch for the treatment of ROU (Table S1 in Supplementary Information).

We designed a 0.5 cm × 0.5 cm dissolvable MN patch base bearing an array of 10 × 10 MNs, each with a height of 350 μm and a base diameter of 200 μm (Fig. 1b). Based on these parameters, we fabricated a resin template of the MN patch with surface projection microstereolithography and cast the drug-loaded ROUMN patch by micromolding (Fig. S2 in Supplementary Information). The resulting MN patch has a flat and flexible base, and the fully cast MNs possess well-defined edges and tips (Fig. 1b).

Dissolution and diffusion test of the dissolvable microneedle patch

As drugs are designed to be dissolved in the base material during fabrication, we performed a dissolution test to evaluate the drug release rate of the dissolvable MNs. Excisions of rat dorsal skin were fixed onto the opening of 1.5 mL Eppendorf centrifuge tubes filled with PBS, and MNs were pressed into the skin excision. Dissolution of the MNs was observed over a time course. The HA MNs dissolved until only the MN bases were left at the 10 s time point, while the gelatin/starch MNs dissolved to the same extent at the 10 min time point (Fig. 1c). The 10 s dissolution window of the HA-based MNs of ROUMN after dermal tissue penetration suggests that as long as the ROUMN patch is not intentionally removed during this working window, it will be able to fully exert its therapeutic effect.

A transdermal diffusion test was then performed to investigate the time window that drug molecules distribute across the dermal tissue. FITC-loaded MNs were pressed into freshly harvested murine dorsal skin and clipped on top of preheated sample flasks of an intelligent transdermal diffusion tester, and a 200 μL sample was extracted for each type of MN at a series of time points (see Methods for details). The concentration of FITC in the aqueous solution extracted at each time point was measured in terms of fluorescence intensity. The results show that at the first time point examined, the amount of fluorescent dye released transdermally by the HA MNs (8342 a.u.) was threefold greater than that released by the gelatin/starch MNs over the same time period (2491 a.u.), and was also 23.6% higher than the plateau value that the gelatin/starch MNs could reach through transdermal diffusion (6750 a.u.). In addition to the faster and more robust drug release, the maximal drug release amount of the HA MNs (13,917 a.u.) was also twice as much as that of the gelatin/starch MNs (Fig. 1d). The superior dissolution and diffusion characteristics make HA the better choice for the base material of ROUMN than gelatin/starch, which possesses comparable mechanical strength.

Mechanical test of the HA microneedle patch in vitro and in vivo

Mechanical strength is essential for the microneedles to penetrate the three layers of oral mucosa and the pseudomembrane covering the ulcer and hence release the drugs throughout the whole depth of the lesion. Therefore, we tested the mechanical properties of the HA MN patch both in vitro and in vivo.

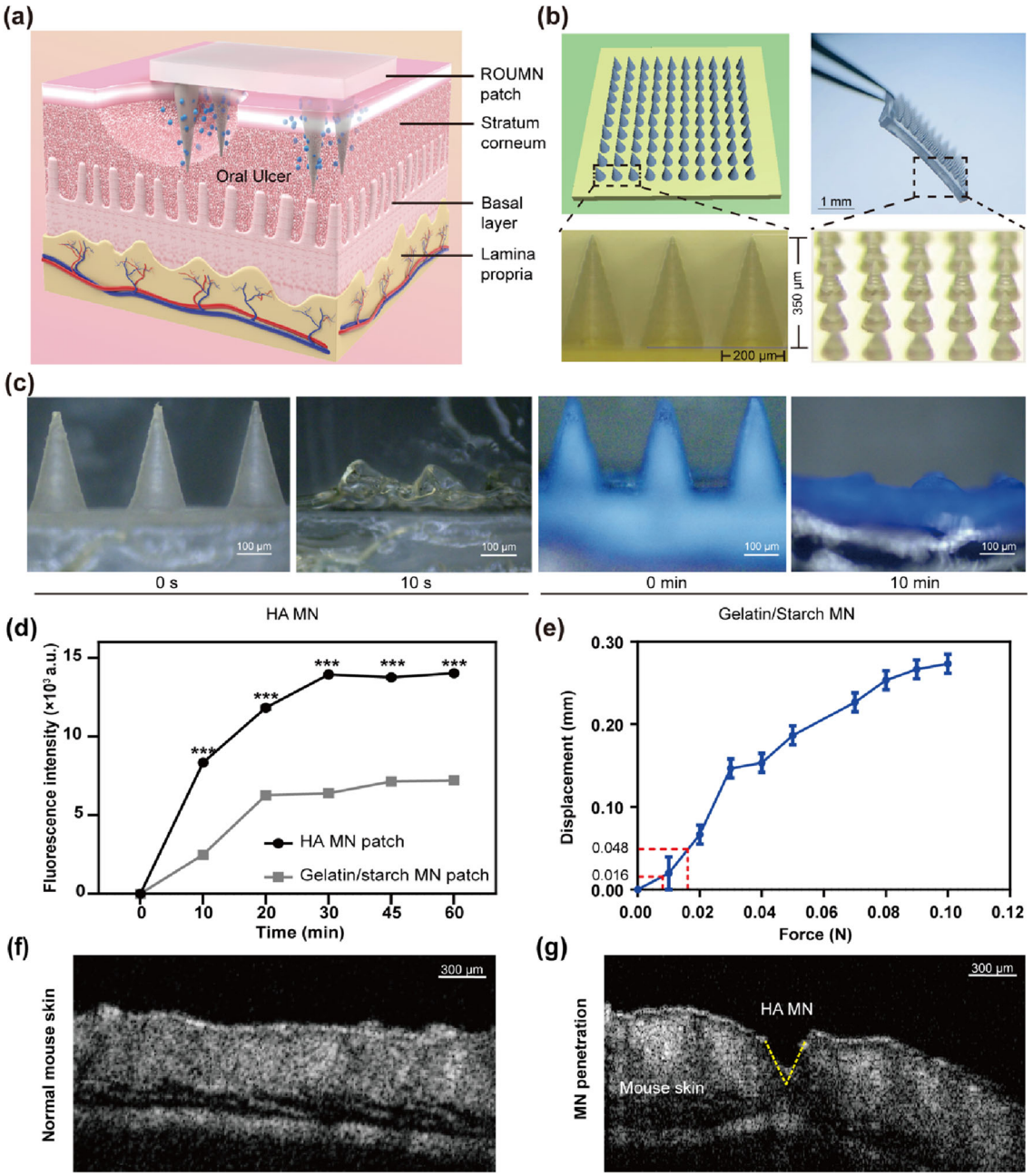

Fig. 1 Overall design and physical characteristics of the recurrent oral ulcer microneedle (ROUMN) patch. **a** Schematic diagram of the multidrug dissolvable microneedle (MN) patch releasing drugs into the oral ulcer. **b** Left: 3D model for fabricating the resin template of the MN patch; inset: side view of the fabricated MNs. Right: ROUMN patch fabricated by micromolding; inset: magnified view of the MN array. **c** Microscopic images of the hyaluronic acid (HA) or gelatin/starch MN patch before and after the dissolution test. **d** Transdermal diffusion curve of the HA MN patch and gelatin/starch MN patch reflected by the intensity of fluorescein isothiocyanate (FITC) released from the dissolved MNs. **e** Mechanical behavior of the HA MN patch in the compression test. The dashed red lines indicate the window of force required to penetrate the buccal mucosa and the mechanical response of the HA MN patch. **f**,**g** Optical coherence tomography (OCT) images showing the mark in murine ventral skin left by HA MN penetration. The yellow dotted "V" indicates the penetrated dermis and disrupted epithelium. Data represent the mean±standard deviation (n=3). ***p<0.001 by Student's t test

The HA MN patch was subjected to a compression test using a universal testing machine. The vertical displacement of the MN tips was recorded against the increasing compressive force applied, and the mechanical behavior of the HA MN patch is plotted as shown in Fig. 1e. The dashed red lines indicate the window of force required to penetrate the buccal mucosa according to the reported (1.54±0.52) MPa

pressure, which translates to 8–16 mN [25]. The corresponding mechanical response of the HA MN patch is a 16–48 μm needle tip displacement, which is less than 14% of the full length of the MNs.

Next, we tested the penetration capability of the dissolvable MNs ex vivo. The HA MN patch was pressed into a rat skin excision, and once the patch was removed, the skin was stained with methylene blue. The arrayed microwounds, as indicated by the darker blue dots on the rat skin, revealed successful penetration and hence good mechanical strength of the HA MNs (Fig. S3 in Supplementary Information).

Since the presentation of mechanical strength ultimately serves to demonstrate that the MNs are able to penetrate the oral mucosa or any tissue surface as the treatment requires, we further verified the mechanical strength of the HA MN patch in vivo by capturing the penetration mark left in skin with optical coherence tomography (OCT). The HA MN patch was pressed into the ventral skin of an anesthetized mouse, where the hair was thoroughly removed. Once the HA MN patch was removed, the marks left by MNs were examined with an OCT machine, and the imaging results are shown in Figs. 1f and 1g. OCT images present the cross-section of the skin along the *Z* axis; the yellow dotted "V" in Fig. 1g indicates the penetrated dermis and disrupted epithelium. The (2.1±0.5) MPa strength required to penetrate murine skin provides clear evidence that the HA-based dissolvable MN patch bears enough mechanical strength for use in the oral mucosa scenario [26].

In vitro anti-inflammatory effect of ROUMN

The proinflammatory cytokine IL-6 has long been studied in association with oral disorders, especially ROU. As serum IL-6 levels were found to be significantly elevated in ROU patients compared with nonpatients, Shen et al. [27] reported that 45% of ROU patient samples surpassed the 2.9 pg/mL baseline serum level of IL-6, confirming the association between serum IL-6 levels and recurrent oral ulcers. Since LPS-induced inflammation is a well-established inflammation model in research studies [28, 29], where LPS induces cellular secretion of IL-6 by binding to TLR4 (Fig. 2a), we adopted this model for in vitro experiments. Cellular expression of IL-6 mRNA was elevated significantly after LPS treatment compared to the control group that was treated with PBS (Fig. 2b), indicating that LPS successfully induced inflammation in the RAEC cell line.

Hence, we evaluated the comprehensive therapeutic effect of the Dex, VC and TH drug combination in the LPS-induced inflammation model. Compared with treatment using Dex alone, treatment with the three drugs combined (ROUMN) exhibited a more remarkable anti-inflammatory effect by suppressing the LPS-induced expression of IL-6 in RAECs (Fig. 2c). Meanwhile, we tested the effect of the drug combination with different concentrations of Dex (10 μM, 50 μM, 100 μM, 1 mM) on the suppression of LPS-induced IL-6 expression by RAEC with ELISA and compared it to the effect of Dex solution alone at the corresponding concentrations. The concentrations of VC and TH varied in proportion to that of Dex for the drug combination group. The results show a steep improvement in the inhibitory effect as the concentration of Dex increased from 10 to 100 μM for both groups; the combination of drugs (ROUMN group) with Dex concentrations at or higher than 50 μM demonstrated a significantly stronger anti-inflammatory effect than treatment using Dex alone. The inhibitory effect of both groups plateaued beyond the Dex concentration of 100 μM, showing a much weaker enhancement as the concentration of Dex increased to the next order of magnitude (Fig. 2d). Since serum TNF-α levels also show a significant difference between ROU patients and nonpatients, although Shen et al. [27] could not confirm the role of TNF-α in the pathology of ROU, we conducted an additional ELISA against LPS-induced TNF-α to evaluate the anti-inflammatory effect of the drugs. Although the inhibitory effect of the drugs towards TNF-α did not show a clear dose-dependent trend as they did for IL-6, the ROUMN drug combination did show a stronger anti-inflammatory effect with statistical significance than Dex alone at Dex concentrations of 50 and 100 μM (Fig. S4 in Supplementary Information).

ROUMN promotes cell proliferation and migration in vitro

In addition to anti-inflammation, promoting cell proliferation to accelerate wound healing is another important aspect of ulcer treatment [30]; therefore, we evaluated cell proliferation after treatment with VC. The CCK-8 assay results showed that the number of live RAECs increased as they were treated with increasing concentrations of VC, verifying the effect of VC in promoting cell proliferation (Fig. 2e). The drug combination of ROUMN with the same concentrations of VC presented a similar dose-dependent promotional pattern and showed a better pro-proliferation effect than VC alone at higher concentrations.

As cell migration from the surrounding healthy oral mucosa tissue towards the ulcerated lesion is part of the healing mechanism [30], it also acts as a factor that determines the speed of healing. We then performed a scratch assay to verify the effect of ROUMN on cell migration. RAECs were allowed to grow into the gap for 24 h after a 24 h incubation with VC alone, ROUMN patch, or drugless complete DMEM (cDMEM). Figures 2f and 2g show that VC alone is able to close the scratch faster in comparison to the control group, yet ROUMN yields an even narrower gap than the VC group, indicating a better ability of the drug combination

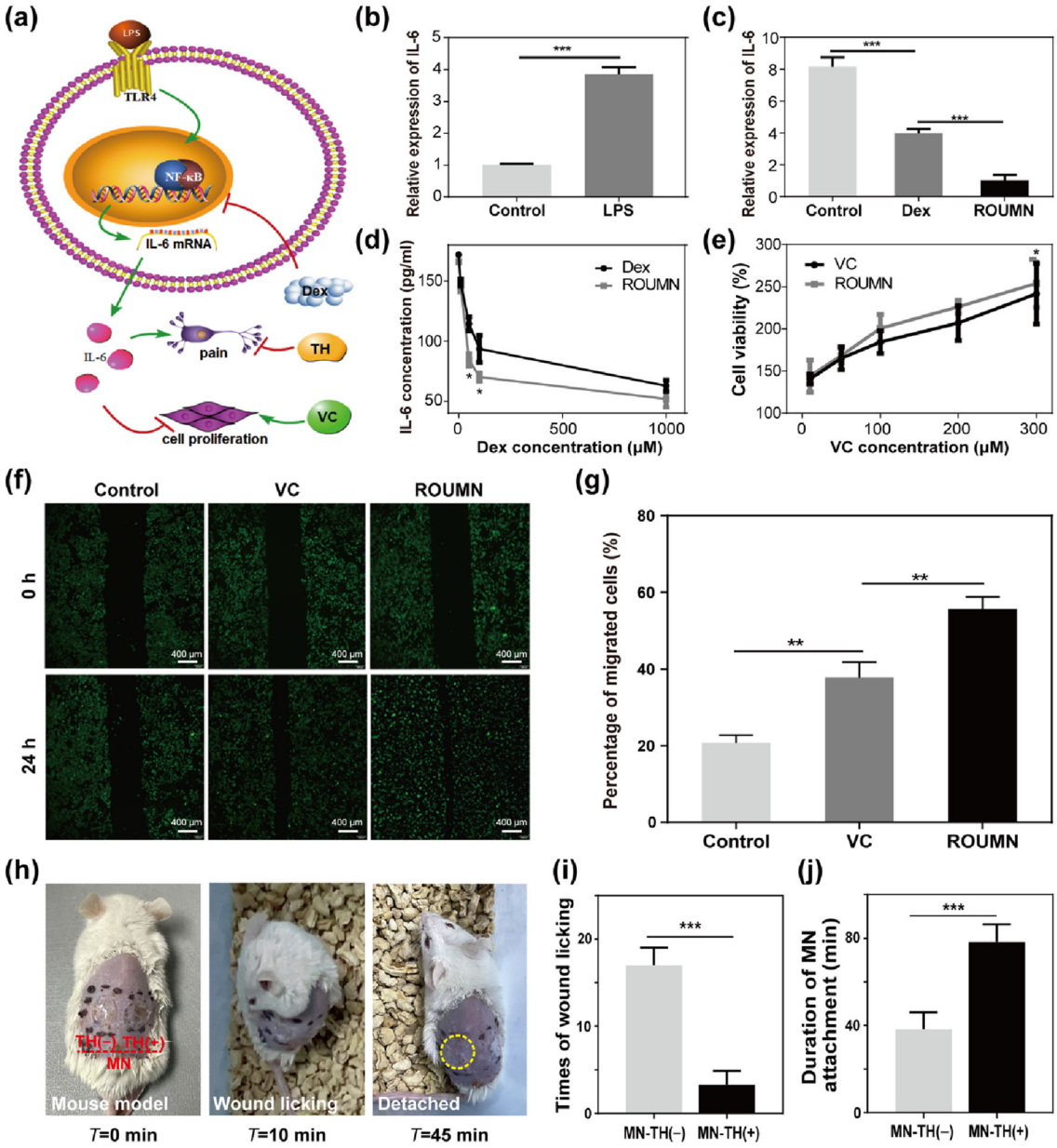

Fig. 2 The anti-inflammatory and pro-proliferative effects of recurrent oral ulcer microneedle (ROUMN) in vitro and the anesthetic effect in vivo. **a** Schematic diagram of lipopolysaccharide (LPS)-induced cellular production of IL-6 and the working mechanism of each drug loaded in the ROUMN patch. Dex: dexamethasone acetate; TH: tetracaine hydrochloride; VC: vitamin C. **b** LPS-induced elevation of IL-6 mRNA levels in rat aortic endothelial cells (RAECs). **c** The suppressing effect of ROUMN on LPS-induced IL-6 mRNA expression in comparison to Dex alone. **d** The suppressing effect of ROUMN on LPS-induced IL-6 protein expression in comparison to Dex alone at various drug concentrations. **e** The promoting effect of the ROUMN drug combination on cell proliferation in comparison to VC alone at various drug concentrations. **f** Fluorescence microscopic images of ROUMN- or VC-treated RAECs proliferating and migrating over the gap over a 24 h period. **g** Statistical analysis of the percentage of migrated cells in (f). **h** Photographs showing one mouse at the beginning, in the middle and at the end of the behavioral test. **i** Statistical results of the number of times the mice licked each wound. **j** Statistical results of the duration that each type of microneedle (MN) patch remained attached to the murine skin. Data represent the mean±standard deviation ($n \geq 3$). ***$p<0.001$, **$p<0.01$, *$p<0.05$ by Student's t test

ROUMN than the single drug VC to promote cell proliferation and migration. The compensatory quantitative cell proliferation assessment comparing the promotional effect of the ROUMN patch to that of single drugs in HA base solution or HA base solution alone revealed that at the cell level, the pro-proliferation effect of the ROUMN patch was attributed to the drug combination and not HA (Fig. S5 in Supplementary Information).

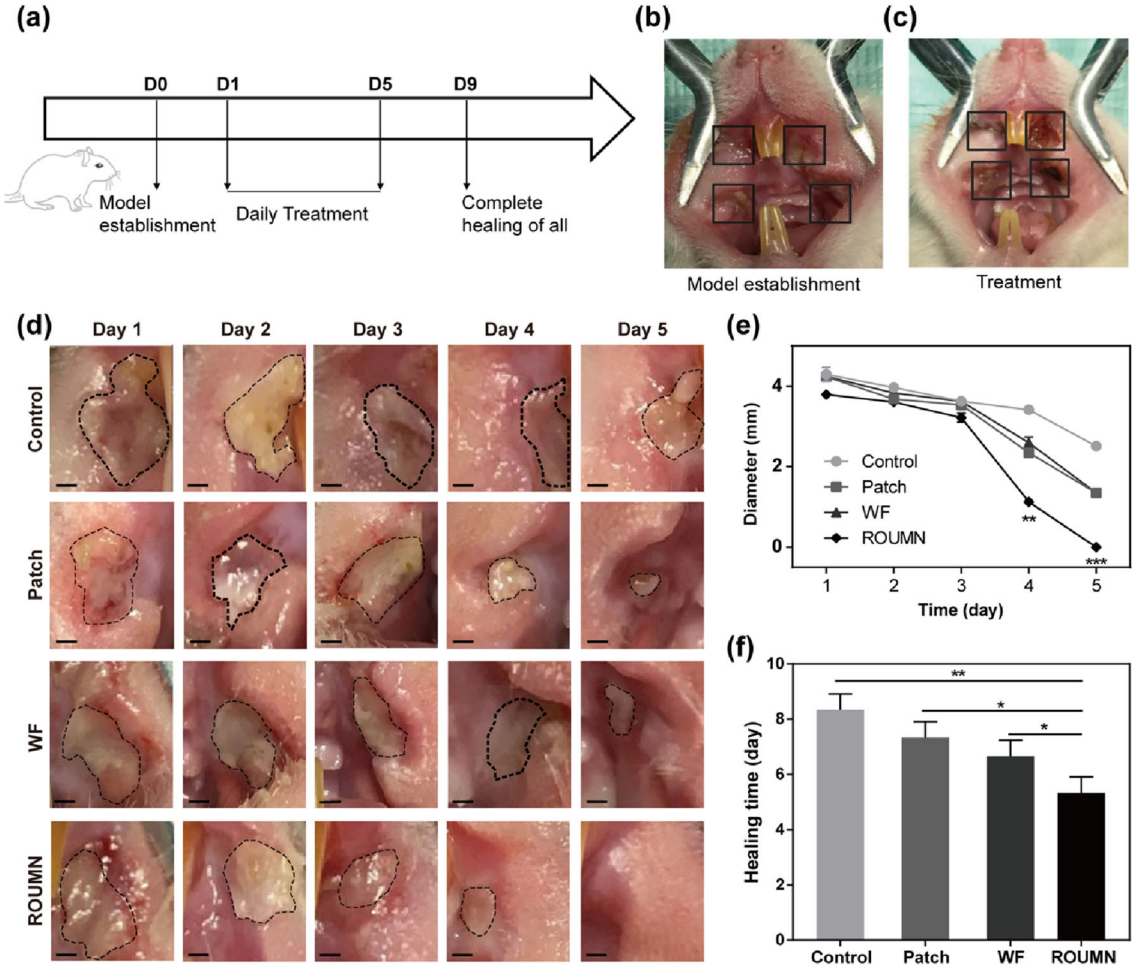

Fig. 3 Overall therapeutic effect of the ROUMN patch on oral ulcers in rats. **a** Timeline of the animal experiment. **b** Photograph of acetic acid-cauterized oral ulcer models in rats. **c** Photograph of the oral ulcers with different treatments applied. Upper left, blank (Control); upper right, ROUMN patch (ROUMN); lower left, drug-loaded hyaluronic acid (HA) patch without microneedles (Patch); lower right, watermelon frost (WF). **d** Photographic records of the morphology of the oral ulcers treated with the four different methods from day 1 to day 5. **e** Changes in the largest diameter of the oral ulcers treated with the four different methods from day 1 to day 5. **f** Total healing time of the oral ulcers treated with the four different methods. Data represent the mean±standard deviation (n=3). ***p<0.001, **p<0.01, *p<0.05 by Student's t test

In vivo anesthetic effect of ROUMN

To evaluate the anesthetic effect of TH in ROUMN, we utilized the murine habit that pain or discomfort triggers mice to lick the site of stimulation and quantified the level of pain or discomfort as the number of times of licking [31]. For the convenience of observation, we reestablished the ulcer model on the dorsal skin of mice with acetic acid cauterization. Three mice were anesthetized in a chamber gassed with isoflurane; once the dorsal skin was exposed with an electric shaver and hair removal cream, two ulcers were created on each mouse on each side of the spine in the waist area while the mouse remained under gas anesthesia through the mask. Before removing the mask, a ROUMN patch (MN-TH(+)) was pressed onto the right-side ulcer, and an MN patch without TH (MN-TH(−)) was pressed onto the left-side ulcer on each mouse (Fig. 2h). Once the mice woke up from anesthesia, the number of times that each mouse licked the ulcer on each side was recorded for 45 min when all TH(−) MN patches detached from the murine skin, and the time points of MN patch detachment were also recorded for both groups. The remarkable difference in the number of times that the mice licked the wound on each side clearly indicates the discomfort caused by the left-side dermal ulcer where the MN patch carries no anesthetic drug, which in turn demonstrates the anesthetic effect of tetracaine hydrochloride (Fig. 2i). The twofold longer duration of ROUMN attachment than the

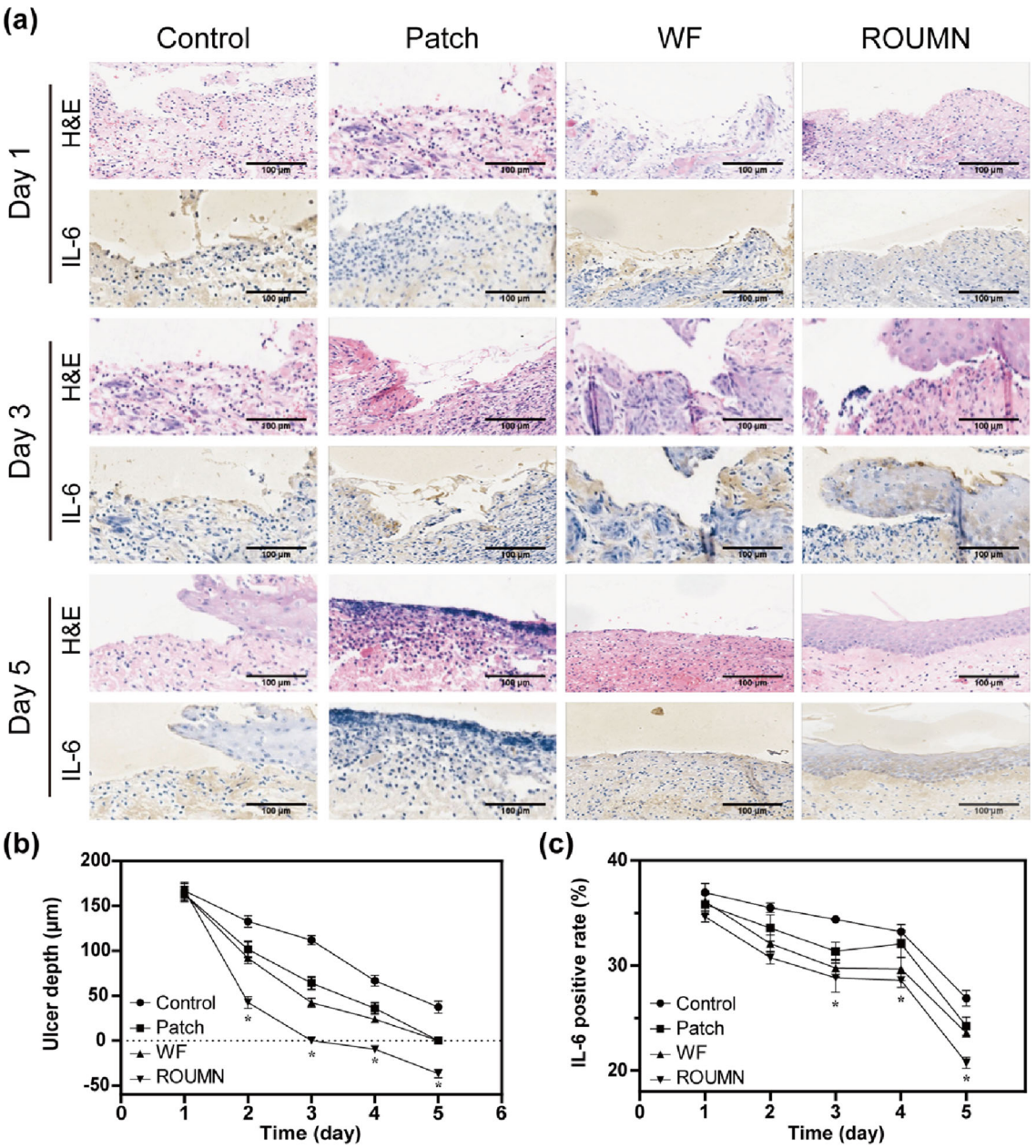

Fig. 4 Clinical analysis showing the promoting effect of ROUMN in oral ulcer healing. **a** Hematoxylin and eosin (H&E) staining and immunohistochemical staining for IL-6 in ulcerated tissue harvested on days 1, 3, and 5. **b** Changes in ulcer depth of the four groups from day 1 to day 5. **c** Statistical analysis of the positive rate of IL-6 in the epithelial layers in the immunostaining images on days 1–5. Data represent the mean±standard deviation (n=3). *p<0.05 by Student's t test

TH(−) MN patch also speaks for the long-lasting anesthetic effect of TH (Fig. 2j).

ROUMN accelerates healing of oral ulcers in vivo

Next, to verify the healing-promoting effect of the ROUMN patch in vivo, we created an oral ulcer model in rats with point application of acetic acid (day 0) and evaluated the healing progress of the ulcerated lesions treated with different drugs for the following 9 days while giving daily treatments once per day on days 1–5 (Fig. 3a). Four ulcers were induced on the buccal mucosa of each rat, where one pair was slightly behind the upper incisors and the other pair was next to the first palatine ruga, as indicated by the black boxes in Fig. 3b. The four ulcers were then left untreated (Control, upper left) or treated with 2 mg ROUMN patch (ROUMN, upper right),

2 mg drug-loaded patch without microneedles (Patch, lower left) or 2 mg watermelon frost, a dark brown powder with reported therapeutic effect to oral ulcers, as a positive control (WF, lower right) (Fig. 3c). The inclusion of a positive control group aims to compare the healing-promoting effect of ROUMN with the most widely applied clinical treatment for recurrent oral ulcers. The effect and use of watermelon frost powder has been well recorded [32, 33]. The method of application of a drug affects its efficiency and thus is part of the treatment; therefore, watermelon frost was applied in its powder form as it is used clinically.

Figures 3d and 3e present the daily healing progress of the four groups from days 1–5 post-treatment. On day 1, the coverage of the ulcerated area by the off-white pseudomembrane was obvious in every group, and three of the four groups showed notable erythematous halos. On day 2, while the pseudomembrane was still visible in all groups, the erythematous halo was alleviated and completely disappeared in the ROUMN group. On day 3, the ulcerated area of the ROUMN group mostly turned pink, resembling the healthy tissue around, in contrast to the clear-edged pseudomembrane in all other groups. Ulcers of the ROUMN group showed a significant decrease in size on day 4 and healed on day 5, while ulceration could still be observed on day 5 for the Patch and WF groups. As we prolonged the observation window until ulcers of all groups healed completely, we concluded that the total healing time of the ROUMN group (5 days) was significantly shorter than that of all other groups (Fig. 3f). These results clearly demonstrate the promoting effect of ROUMN in oral ulcer healing.

To further analyze the healing mechanism of ROUMN-treated oral ulcers, we harvested the tissue of the ulceration areas 1, 3, and 5 days post-treatment for H&E staining and immunohistochemistry staining against IL-6 (Fig. 4a). On day 3, the depth of the ulcerated lesion in the ROUMN group decreased significantly from day 1, and a thin basal layer could also be observed on top of the lesion, while the lesions of all other groups remained a depth down to the lamina propria. On day 5, the ulcerated lesion in the ROUMN group was covered with a complete basal layer, and the more superior epithelial layers (i.e., stratum spinosum, stratum granulosum, and stratum corneum) also fully formed over the lesion; lesions of the patch and WF groups developed a thin basal layer, and the control group ulcer still showed an exposed lamina propria. The analysis of ulcer depth showed a statistically significant difference between the daily measurements of the ROUMN group and those of all other groups after only 1 day of treatment (Fig. 4b). Image analysis of the IL-6 immunostaining revealed that the positive rate of IL-6 in the mucosal layers above the lamina propria was the lowest in the ROUMN group, indicating that the anti-inflammatory effect of the ROUMN patch contributes to its overall promoting effect on oral ulcer healing (Fig. 4c).

Conclusions

In this work, we presented a multidrug dissolvable microneedle patch (ROUMN patch) fabricated through micromolding for the treatment of recurrent oral ulcers. The 350-μm-long HA-based MNs bear enough mechanical strength to effectively penetrate the pseudomembrane covering the oral ulcer. The ROUMNs are able to fully dissolve within 10 s and rapidly release dexamethasone, vitamin C and tetracaine into the ulcerated lesion. In vitro experiments verified that this drug combination of ROUMN is more effective at reducing inflammation than dexamethasone alone and at promoting cell proliferation and migration than vitamin C alone. The acetic acid-cauterized rat oral ulcer model demonstrated the superior healing-promoting effect of ROUMN through the shortened healing time compared to treatment with an existing drug for oral ulcers. The fast release of anesthetic tetracaine and the painless application of MNs should ensure good patient compliance; together with the enhanced therapeutic effect of the drug combination, these advantages should endow ROUMNs with high translational value and hence broad application prospects in the treatment of recurrent oral ulcers.

Supplementary Information The online version contains supplementary material available at https://doi.org/10.1007/s42242-022-00221-3.

Acknowledgements This work was supported by the National Natural Science Foundation of China (Nos. 62003023, 32071407, 52073138, 52003018 and 52003019), Beijing Natural Science Foundation (No. 7212204), and Beijing Advanced Innovation Center for Biomedical Engineering and Beihang University.

Author contributions LQC and JL conceived the project, collected funding, and guided the experiments. YYH guided the animal experiments. YQW designed the experiments and provided guidance for the study. Microneedle design and fabrication were done by AAS. In vitro experiments and data collection were done by AAS and XRJ. In vivo experiments and data collection were done by YQW and SSY. Manuscript composition and revision were done by YQW and XRJ. LL, MZY and FSZ helped with some experiments.

Declarations

Conflict of interest The authors declare that there is no conflict of interest.

Ethical approval This project was approved by Xiamen University Animal Care and Use Committee. The approval code number is XMU-LAC20210063. All institutional and national guidelines for the care and use of laboratory animals were followed.

References

1. Natah SS, Konttinen YT, Enattah NS et al (2004) Recurrent aphthous ulcers today: a review of the growing knowledge. Int J Oral Maxillofac Surg 33:221–234. https://doi.org/10.1006/ijom.2002.0446

2. Shah K, Guarderas J, Krishnaswamy G (2016) Aphthous stomatitis. Ann Allergy Asthma Immunol 117(4):341–343. https://doi.org/10.1016/j.anai.2016.07.005
3. Muñoz-Corcuera M, Esparza-Gómez G, González-Moles MA et al (2009) Oral ulcers: clinical aspects. A tool for dermatologists. Part II. Chronic ulcers. Clin Exp Dermatol 34(4):456–461. https://doi.org/10.1111/j.1365-2230.2009.03220.x
4. Fitzpatrick SG, Cohen DM, Clark AN (2019) Ulcerated lesion of the oral mucosa: clinical and histologic review. Head Neck Pathol 13(1):91–102. https://doi.org/10.1007/s12105-018-0981-8
5. Edgar NR, Saleh D, Miller R (2017) Recurrent aphthous stomatitis: a review. J Clin Aesthet Dermatol 10(3):26–36
6. Liu C, Zhou Z, Liu G et al (2012) Efficacy and safety of dexamethasone ointment on recurrent aphthous ulceration. Am J Med 125(3):292–301. https://doi.org/10.1016/j.amjmed.2011.09.011
7. Liu J, Zeng X, Chen Q et al (2006) An evaluation on the efficacy and safety of amlexanox oral adhesive tablets in the treatment of recurrent minor aphthous ulceration in a Chinese cohort: a randomized, double-blind, vehicle-controlled, unparallel multicenter clinical trial. Oral Surg Oral Med Oral Pathol Oral Radiol Endod 102(4):475–481. https://doi.org/10.1016/j.tripleo.2005.12.014
8. Zhang C, Liu Y, Li W et al (2019) Mucoadhesive buccal film containing ornidazole and dexamethasone for oral ulcers: in vitro and in vivo studies. Pharm Dev Technol 24(1):118–126. https://doi.org/10.1080/10837450.2018.1428814
9. Zhao X, Li X, Zhang P et al (2018) Tip-loaded fast-dissolving microneedle patches for photodynamic therapy of subcutaneous tumor. J Contr Release 286:201–209. https://doi.org/10.1016/j.jconrel.2018.07.038
10. Yang H, Wu X, Zhou Z et al (2019) Enhanced transdermal lymphatic delivery of doxorubicin via hyaluronic acid based transfersomes/microneedle complex for tumor metastasis therapy. Int J Biol Macromo 125:9–16. https://doi.org/10.1016/j.ijbiomac.2018.11.230
11. Bok M, Zhao ZZ, Jeon S et al (2020) Ultrasonically and iontophoretically enhanced drug-delivery system based on dissolving microneedle patches. Sci Rep 10(1):2027. https://doi.org/10.1038/s41598-020-58822-w
12. Snetkov P, Zakharova K, Morozkina S et al (2020) Hyaluronic acid: the influence of molecular weight on structural, physical, physicochemical, and degradable properties of biopolymer. Polymers 12(8):1800. https://doi.org/10.3390/polym12081800
13. Saha I, Rai VK (2021) Hyaluroic acid based microneedle array: recent application in drug delivery and cosmetology. Carbohydr Polym 267:118168. https://doi.org/10.3390/polym12081800
14. Ghazi K, Deng-Pichon U, Warnet JM et al (2012) Hyaluronan fragments improve wound healing on in vitro cutaneous model through P2X7 purinoreceptor basal activation: role of molecular weight. PLoS ONE 7(11):e48351. https://doi.org/10.1371/journal.pone.0048351
15. Ruan J, Li D, Tao H et al (2018) Effects of dexamethasone on the EGF mRNA levels and inflammatory factors in rabbits with oral ulcers. Pharm Bioprocess 6(3):119–125
16. Tu H, Zhang D, Barksdale AN et al (2020) Dexamethasone improves wound healing by decreased inflammation and increased vasculogenesis in mouse skin frostbite model. Wilderness Environ Med 31(4):407–417. https://doi.org/10.1016/j.wem.2020.07.003
17. Li X, Tang L, Lin YF et al (2018) Role of vitamin C in wound healing after dental implant surgery in patients treated with bone grafts and patients with chronic periodontitis. Clin Implant Dent Relat Res 20(5):793–798. https://doi.org/10.1111/cid.12647
18. Gunton JB, Girgis CM, Lau T et al (2021) Vitamin C improves healing of foot ulcers: a randomized, double-blind, placebo-controlled trial. Br J Nutr 126(10):1451–1458. https://doi.org/10.1017/S0007114520003815
19. Palmieri B, Vadalà M, Laurino C (2019) Nutrition in wound healing: investigation of the molecular mechanisms, a narrative review. J Wound Care 28(10):683–693. https://doi.org/10.12968/jowc.2019.28.10.683
20. O'Brien L, Taddio A, Lyszkiewicz DA et al (2005) A critical review of the topical local anesthetic amethocaine (Ametop™) for pediatric pain. Pediatr Drugs 7(1):41–54. https://doi.org/10.2165/00148581-200507010-00004
21. McGee DL (2017) Local and topical anesthesia. In: Roberts and Hedges' Clinical Procedures in Emergency Medicine and Acute Care (7th Ed.). Elsevier, Amsterdam, pp 523-544.e3
22. Duarah S, Sharma M, Wen J (2019) Recent advances in microneedle-based drug delivery: special emphasis on its use in paediatric population. Eur J Pharm Biopharm 136:48–69. https://doi.org/10.1016/j.ejpb.2019.01.005
23. Hackethal J, Iredahl F, Henricson J et al (2021) Microvascular effects of microneedle application. Skin Res Technol 27(2):121–125. https://doi.org/10.1111/srt.12918
24. Bora P, Kumar L, Bansal AK (2008) Microneedle technology for advanced drug delivery: evolving vistas. Niper Crips 9(1):7–10
25. Choi JE, Zwirner J, Ramani RS et al (2020) Mechanical properties of human oral mucosa tissues are site dependent: a combined biomechanical, histological and ultrastructural approach. Clin Exp Dent Res 6:602–611. https://doi.org/10.1002/cre2.305
26. Bermudez DM, Herdrich BJ, Xu JW et al (2011) Impaired biomechanical properties of diabetic skin implications in pathogenesis of diabetic wound complications. Am J Pathol 178(5):2215–2223. https://doi.org/10.1016/j.ajpath.2011.01.015
27. Shen C, Ye W, Gong L et al (2021) Serum interleukin-6, interleukin-17A, and tumor necrosis factor-alpha in patients with recurrent aphthous stomatitis. J Oral Pathol Med 50(4):418–423. https://doi.org/10.1111/jop.13158
28. Kaewduangduen W, Visitchanakun P, Saisorn W et al (2022) Blood bacteria-free DNA in septic mice enhances LPS-induced inflammation in mice through macrophage response. Int J Mol Sci 23(3):1907. https://doi.org/10.3390/ijms23031907
29. Yang L, Wu G, Wu Q et al (2022) METTL3 overexpression aggravates LPS-induced cellular inflammation in mouse intestinal epithelial cells and DSS-induced IBD in mice. Cell Death Discov 8(1):62. https://doi.org/10.1038/s41420-022-00849-1
30. Velnar T, Bailey T, Smrkolj V (2009) The wound healing process: an overview of the cellular and molecular mechanisms. J Int Med Res 37(5):1528–1542. https://doi.org/10.1177/147323000903700531
31. Lu J, Wang Z, Ren M et al (2016) Antibacterial effect of gallic acid against aeromonas hydrophila and aeromonas sobria through damaging membrane integrity. Current Pharm Biotechnol 17(13):1153–1158. https://doi.org/10.2174/1389201017666161022235759
32. Zhao X, He X, Zhong X (2016) Anti-inflammatory and in-vitro antibacterial activities of Traditional Chinese Medicine Formula Qingdaisan. BMC Complement Altern Med 16(1):503. https://doi.org/10.1186/s12906-016-1475-4
33. Liu Z, Dou H (2022) Effects of four types of watermelon frost combination medications for the treatment of oral ulcers: a network meta-analysis. J Healthc Eng 2022:2712403. https://doi.org/10.1155/2022/2712403